# Influence of yttrium doping on ZnO nanoparticles for enhanced photocatalytic degradation of methylene blue

T. Rungsawang[a], S. Sujinnapram[b], S. Nilphai[c], S. Wongrerkdee[b,*]
[a]*Department of Chemistry, Faculty of Liberal Arts and Science, Kasetsart University Kamphaeng Saen Campus, Nakhon Pathom 73140, Thailand*
[b]*Department of Physics, Faculty of Liberal Arts and Science, Kasetsart University Kamphaeng Saen Campus, Nakhon Pathom 73140, Thailand*
[c]*Physics Program, Department of Science and Technology, Faculty of Liberal Arts and Science, Roi Et Rajabhat University, Thailand*

In this work, Y-doped ZnO nanoparticles were precipitately synthesized for various yttrium molar percentage values ranging from 0 to 5%, and then utilized as photocatalysts to demonstrate methylene blue degradation. Morphology shows that the particle size of pure ZnO is 113.77±33.26 nm, which is reduced to the minimum value less than one-third for the Y-doped ZnO samples. As a result, surface-to-volume ratios of Y-doped ZnO samples have successfully increased due to their decreased size. This decrease in particle size is consistent with the small crystalline size, primarily due to low crystallization in the presence of yttrium doping. However, the expansion of the crystal structure is observed. Chemical surface structures point to the major vibration of ZnO. However, some carbon-relating groups remain to appear. Optical property reveals similar trends for all Y-doped ZnO samples. The estimated band gap energy ($E_g$) was reduced to the minimum value for the 4 mol% condition. For use as a photocatalyst, the appropriate Y-doped ZnO for 4 mol% yttrium doping presents the maximum degradation efficiency of 61.19%. The improvement in photocatalytic degradation is caused by the synergy of decreased particle size and reduced $E_g$. Therefore, yttrium plays a role to decrease particle size and reduce $E_g$ of Y-doped ZnO materials, thus leading to enhance photocatalytic performance.

(Received July 26, 2021; Accepted October 4, 2021)

*Keywords:* Yttrium, ZnO, Nanoparticles, Photocatalytic degradation, Methylene blue

## 1. Introduction

Pollution in water resources is a serious problem that has harmed both human health and the surrounding natural system. Toxic chemicals are the primary contaminants that continue to pollute the surrounding land, air, and water. In water, chemicals cause wastewater, which is a worrying issue and has a large-scale impact on the environment, especially if it is transported to natural rivers. Photocatalytic degradation is an effective method to reduce chemical residue, due to its simple and flexible uses [1]. Photocatalytic degradation is based on two fundamental processes, namely, photoactivation and degradation. Photoactivation occurs when photocatalysts absorb energy from incident light for generating electron-hole pairs, which are continuously transferred to the photocatalyst's surface. The pairs react with chemical residue for mineral transformation during the degradation process.

Several semiconductor materials such as $TiO_2$, CuO, $SnO_2$, and ZnO have been investigated as photocatalysts [2-4]. Among these, ZnO is an interesting one, primarily due to its stability and unique opto-electronic properties. ZnO has a large band gap ($E_g$) of around 3.70 eV that can be specifically activated by ultra-violet (UV) light; a high carrier mobility for rapidly transferring electron-hole pairs to the material's surface; and a relatively stable chemical structure [4]. Furthermore, ZnO offers benefits in a variety of nano-structural fabrications. To improve the photocatalytic activity of ZnO, it has been demonstrated with several improvements in charge separations, lifetimes, and surface areas. Phopayu *et al*. modified ZnO by using graphene quantum

* Corresponding author: sutthipoj.s@gmail.com

dots (GQDs) doping for extending the crystalline structure of the GQDs-ZnO nanocomposites [5]. The extended structure has reducing grain boundary density, thus causing a lower electron-hole pair recombination at the grain boundary. This behavior plays the role to increase the lifetime for electron-hole pair movement at surfaces of the GQDs-ZnO, which results in high photocatalytic performance for commercial glyphosate degradation. Bozetine *et al*. presented the simple and green synthesis of ZnO/carbon quantum dots (CQDs)/Ag nanoparticles (NPs) nanocomposites for photocatalytic application. The nanocomposites exhibited excellent photocatalytic performance due to the improved charge separation efficiency and increased surface area [4]. The charge separation improved because electrons can easily be transferred in the nanocomposites caused by the energy level adjustment for heterojunction interfaces. This result is in line with several composite structures reported elsewhere [6-8]. For the increased surface area, it was described by the attachment of small CQDs or Ag NPs on the ZnO surface. The improved charge separation efficiency and increased surface areas of ZnO/CQDs/AgNPs nanocomposites synergistically enhanced the photocatalytic degradation of methylene blue (MB). Yu *et al*. developed ZnO/biochar nanocomposites using a facile ball-milling method as a photocatalyst [9]. The nanocomposites exhibited increased mesopore and macropore structures compared to pure ZnO. In photocatalyst applications, the degradation efficiency of MB peaked at 95.19% under visible light activation. The improvement in degradation efficiency was caused by the combination of adsorption and photocatalysis processes. Wang *et al*. prepared Ce-doped ZnO using a simple solution method [10]. They found that Ce-doping caused a decrease in particle size and $E_g$ values. These results synergistically function to improve photocatalytic activity, which subsequently enhanced the degradation efficiency of MB.

In the current work, Y-doped ZnO photocatalysts were synthesized from a mixture of zinc nitrate and yttrium nitrate. To examine the effect of yttrium on structural, chemical, and optical characteristics, the yttrium nitrate was changed in the molar percentage ranging from 0 to 5%. The characteristics of Y-doped ZnO were investigated and analyzed. The Y-doped ZnO was use as a photocatalyst for MB degradation. The photocatalytic degradation efficiencies were calculated based on the absorbance measurement to evaluate the appropriate yttrium content of Y-doped ZnO for optimum MB degradation.

## 2. Experimental details

Y-doped ZnO was synthesized by dissolving zinc nitrate hexahydrate with 0-5 mol% yttrium nitrate in de-ionized (DI) water at a concentration of 0.1 M. The mixture was then stirred and heated at 70°C for 30 min. To precipitate as Y-doped ZnO, 0.2 M sodium hydrogen carbonate solution was poured into the mixture under continuous stirring and heating to obtain a precipitated solution. After it cooled down to room temperature, the precipitated solution was filtered overnight to obtain a white-precursor product. The product was then treated by drying at 70°C for 3 h, grinding for 30 min, and calcining at 600°C for 6 h, respectively. The resulting product was grounded again to obtain the Y-ZnO product.

The morphology of Y-doped ZnO was observed by using a scanning electron microscope (SEM). The SEM image was analyzed by using Image-J software for particle size measurement. The crystalline structure was investigated based on the X-ray diffraction (XRD) pattern. The chemical surface structure was detected by using Fourier-transform infrared (FT-IR) spectrometer operated in a wavenumber range of 450 to 4000 $cm^{-1}$. The diffuse reflectance absorption spectra were monitored using an ultraviolet-visible-near infrared (UV-Vis-NIR) spectrophotometer, to study the optical properties of Y-doped ZnO; the optical band gap ($E_g$) was estimated based on the optical spectra.

For photocatalytic application, all Y-doped ZnO samples were used as photocatalysts for MB degradation. The MB solution was prepared by dissolving 15 mg of MB into 1 L of DI water and stirred for 30 min, in the dark. The Y-doped ZnO was dispersed into the MB solution by sonicating for 5 min. Prior to the photocatalytic test, the dispersion was left in the dark for 30 min for adsorption/desorption equilibrium. Then, UV lamps ($\lambda$~365 nm, 1.6 $mW/cm^2$) were turned on

to boot the photocatalytic activity of Y-doped ZnO for MB degradation. To evaluate the photocatalytic efficiency, the optical absorbance of the degraded MB solution was measured and analyzed.

## 3. Results and discussion

Fig. 1 depicts the morphologies of Y-doped ZnO precipitated for various yttrium molar percentages. The relative smaller particles are observed for all Y-doped ZnO samples in comparison to pure ZnO. To estimate the particle size, Image-J software was used, and the particle size was plotted in Fig. 2. The particle size of pure ZnO reveals the largest value with a wide distribution of 113.77±33.26 nm. For the Y-doped ZnO samples, the particle size reduces to less than one-third of the pure ZnO and features better regular distribution. This behavior occurs because the reaction between $Zn^{2+}$ and $OH^{-}$ ions is intercepted by $Y^{3+}$ ions. Therefore, the presence of yttrium content results in the short reaction rate of precipitated ZnO, which causes the formation of small sized particles. As a result, surface-to-volume ratios of Y-doped ZnO samples have successfully increased due to their decreased size.

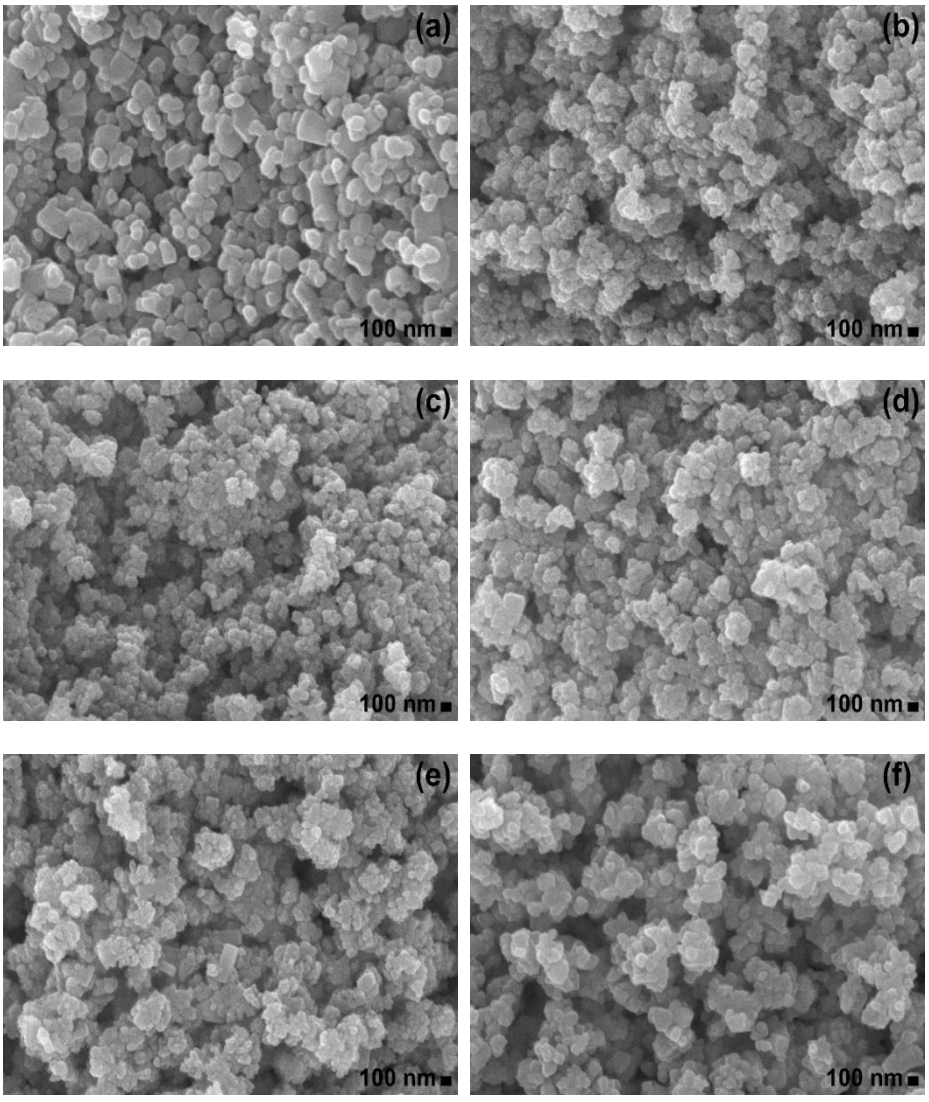


*Fig. 1 Morphology of Y-doped ZnO for various yttrium molar percentages of (a) 0%, (b) 1%, (c) 2%, (d) 3%, (e) 4%, and (f) 5%.*

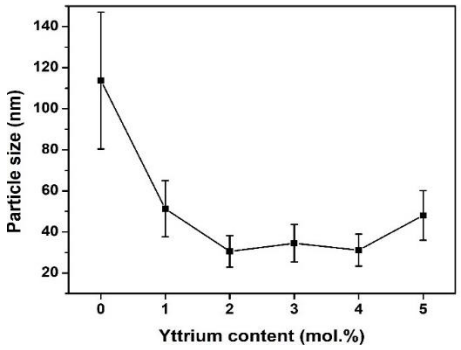


*Fig. 2 Particle size of Y-doped ZnO for various yttrium molar percentages.*

Fig. 3 presents the XRD patterns of the Y-doped ZnO for various yttrium molar percentages. The XRD results exhibit similar diffraction patterns for all samples, which corresponds to the hexagonal wurtzite structure of ZnO, in agreement with the standard JCPDS card no. 36-1451 [11]. To investigate the influence of yttrium content on the crystallization of Y-doped ZnO, the crystal characteristics including crystalline size (D), lattice constant (a and c), and d-spacing (d) were calculated according to Eqs. (1) – (4) [12-14].

$$D = \frac{k\lambda}{\beta \cos\theta} \tag{1}$$

$$a = \frac{\lambda}{\sqrt{3}\sin\theta} \tag{2}$$

$$c = \frac{\lambda}{\sin\theta} \tag{3}$$

$$2d \sin\theta = n\lambda \tag{4}$$

where k is the constant of the XRD measurement system (0.89), $\lambda$ is the wavelength of the X-ray source (1.5406 Å), $\beta$ is the full-width at the half-maximum (FWHM) intensity, $\theta$ is the diffraction angle, and n is 1 for the first-order diffraction. The crystalline size was calculated from the three major peaks of (100), (002), and (101) plans. The (100) and (002) plans were used to calculate the lattice constants a and c, respectively, as well as the d-spacing $d_{100}$ and $d_{002}$. The calculated characteristic values are listed in Table 1. The average crystal size decreases for the Y-doped ZnO in comparison to pure ZnO, which seems to have a similar pattern of particle size, confirming the rapid precipitation with low crystallization for the presence of yttrium contents. On the other hand, lattice constants (a and c) and d-spacing values increased for the Y-doped ZnO samples. These results are due to the substitution of the smaller $Zn^{2+}$ ions by the larger $Y^{3+}$ ions in the ZnO unit cell, which causes the extension for the Y-doped ZnO samples in comparison to pure ZnO [15].

Fig. 4 shows FT-IR results of the Y-doped ZnO for various yttrium molar percentage values. The major FT-IR peaks that correspond to the Zn–O stretching vibration were detected at 467, 473, 481, 482, 479, and 470 $cm^{-1}$ for the yttrium molar percentages of 0, 1, 2, 3, 4, and 5%, respectively. It was observed that the FT-IR peaks shift to a higher wavenumber for Y-doped ZnO samples in comparison to pure ZnO which can be interpreted to the effect of incorporation of Y into the Zn–O lattice [16]. This result confirms the substitution effect, which is in line with the XRD results. Note that the observed peaks at around 1367 and 2359 $cm^{-1}$ are assigned to the C–O stretching and $CO_2$ groups [17, 18], respectively, which implies the existence of chemical surface defects.

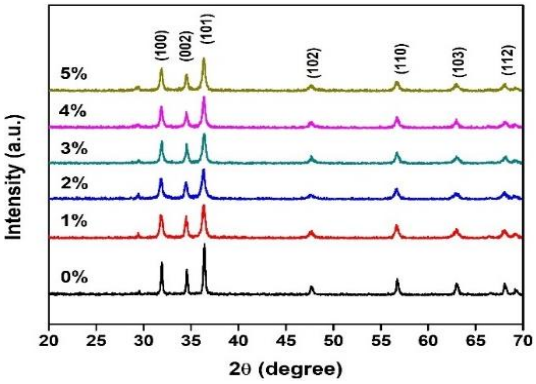


*Fig. 3. XRD pattern of Y-doped ZnO for various yttrium molar percentages.*

*Table 1. Crystal characteristics of Y-doped ZnO for various yttrium molar percentages.*

| Y mol% | D (nm) | a (Å) | c (Å) | $d_{100}$ | $d_{002}$ |
|---|---|---|---|---|---|
| 0 | 38.11±3.62 | 3.2341 | 5.1846 | 2.8007 | 2.5923 |
| 1 | 22.71±2.63 | 3.2403 | 5.1965 | 2.8061 | 2.5982 |
| 2 | 22.07±2.96 | 3.2429 | 5.1983 | 2.8084 | 2.5991 |
| 3 | 23.55±3.02 | 3.2359 | 5.1855 | 2.8023 | 2.5927 |
| 4 | 24.23±1.24 | 3.2392 | 5.1911 | 2.8051 | 2.5955 |
| 5 | 25.23±3.27 | 3.2393 | 5.1910 | 2.8053 | 2.5955 |

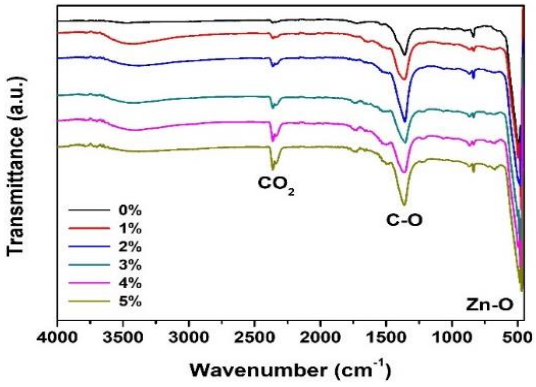


*Fig. 4. FT–IR spectra of Y-doped ZnO for various yttrium molar percentages.*

Fig. 5 shows the optical absorbance spectra of Y-doped ZnO measured at a wavelength range of 200 – 800 nm. The absorbance spectra reveal a low response for the visible region, but a strong absorbance is observed across the UV region. To estimate the optical band gap ($E_g$), the Tauc's relation was plotted as shown in the inset of Fig. 5, according to Eq. (5) [14].

$$\alpha h\nu = A\left(h\nu - E_g\right)^n \tag{5}$$

where α and A are constants, h is the Plank's constant, ν is the frequency, and n is ½ for direct band gap semiconductors as for ZnO. For $E_g$ estimation, an extrapolation from the linear part up to the hν-axis was fitted. Then, the $E_g$ value be traced from the interception, as shown in the inset of

Fig. 5. The $E_g$ values are in the range of 3.2196-3.2265 eV, which result in insignificant changes. The $E_g$ results also specify that all Y-doped ZnO samples respond to UV energy, which can be suitable as a photocatalyst under UV irradiation. Note that for the Y-doped ZnO sample for 4 mol% of yttrium doping, $E_g$ reveals the minimum value, indicating a low energy requirement for booting the photocatalytic activity.

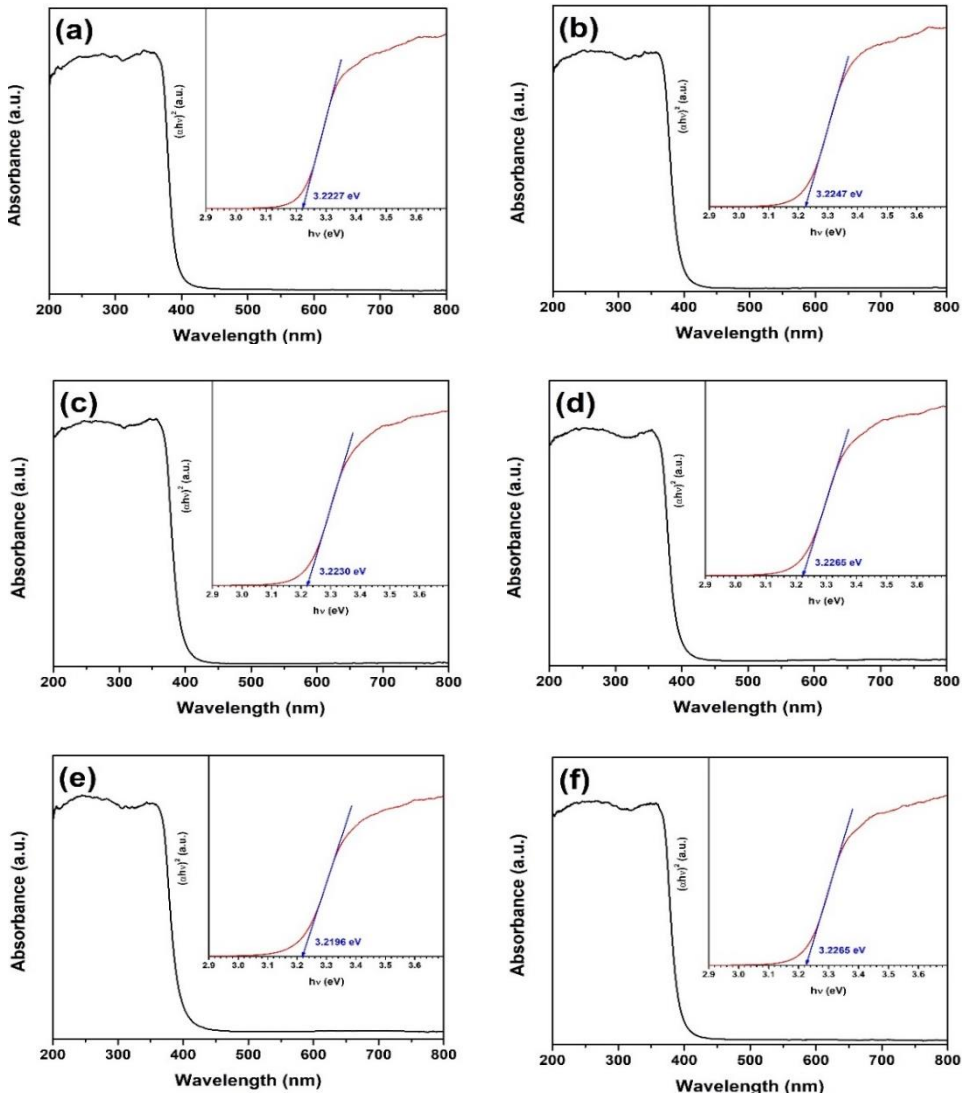


*Fig. 5. Optical absorbance of Y-doped ZnO for various yttrium molar percentages, and the inset figure of Tauc plots.*

All Y-doped ZnO samples were then used as a photocatalyst to degrade MB for the photocatalytic test. Fig. 6 shows the absorbance of MB after being degraded for 0-150 min of irradiation time. The absorbance spectra of MB decrease after photocatalytic degradation for all Y-doped ZnO samples. This result indicates that Y-doped ZnO plays the role to degrade MB under photocatalytic activity. To evaluate the appropriate Y-doped ZnO sample, the degradation efficiency was calculated by comparing the absorbance of MB for 150 min irradiation time with that for the initial irradiation time, according to Eq. (6) [19].

$$\text{Degradation efficiency} = 1 - \frac{A}{A_0} \tag{5}$$

where $A_0$ and A are absorbance of MB at a wavelength of 660 nm for the initial and final irradiation times, respectively. Fig. 7 shows that the degradation efficiency increases with increasing yttrium molar percentages for 0-4 mol%. The degradation efficiency reaches the maximum value of 61.19% for the 4 mol% of yttrium doping. For yttrium doping at 5 mol%, the degradation efficiency is again decreased to a lower value. It can be interpreted that Y-doped ZnO for 4 mol% of yttrium ding is the best photocatalyst in this case. This behavior is due to the synergy of decreased particle size and reduced $E_g$. The decrease in particle size of Y-doped ZnO can offer a high surface area for the chemical reaction between MB and Y-doped ZnO during the photocatalytic activity. The reduced $E_g$ value of Y-doped ZnO can also the facilitate photocatalytic activity, since it requires a comparatively lower activated-energy for photocatalytic activation, in comparison to pure ZnO.

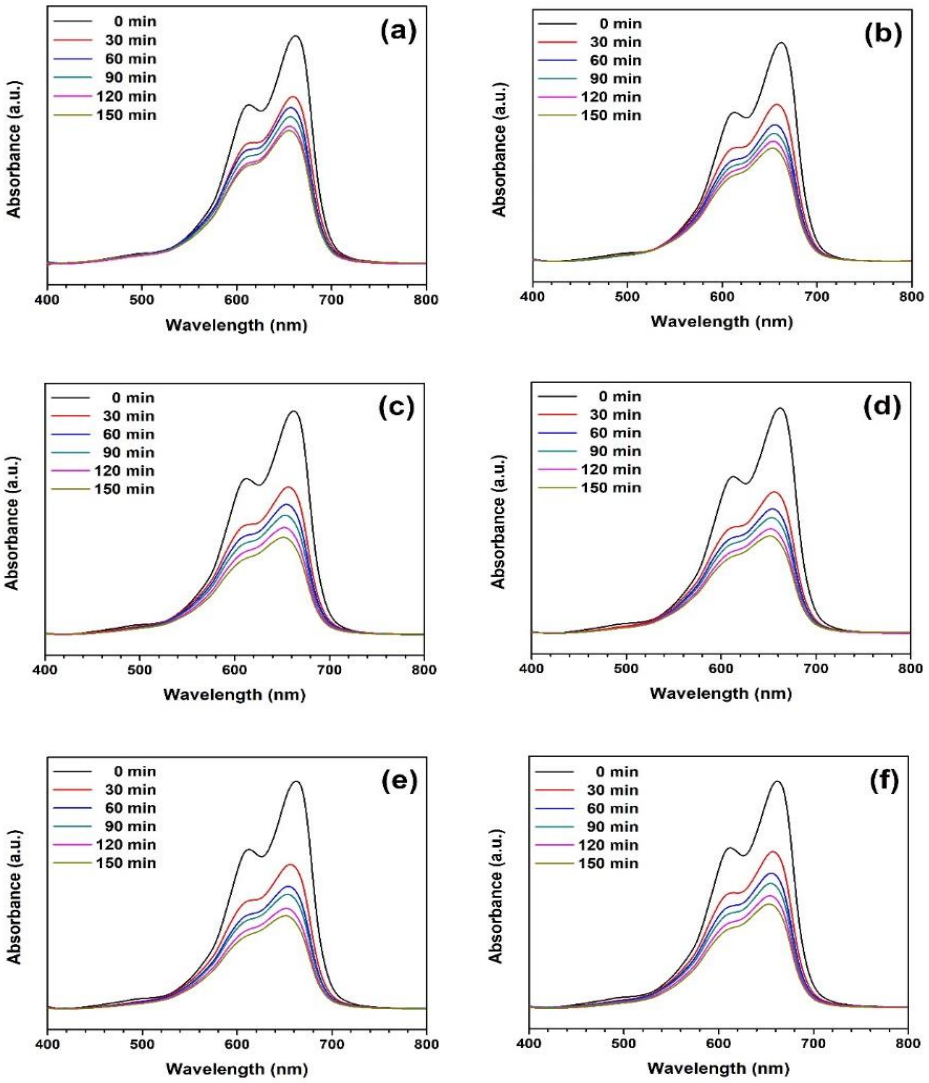


*Fig. 6. Absorbance of methylene blue degraded under UV illumination for 0-150 min using Y-doped ZnO photocatalyst for various yttrium molar percentages of (a) 0, (b) 1, (c) 2, (d) 3, (e) 4, and (f) 5%.*

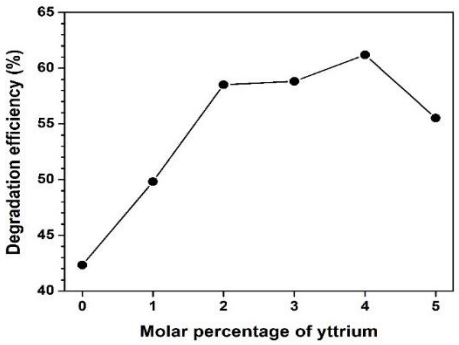


*Fig. 7. Degradation efficiency of methylene blue using Y-doped ZnO photocatalyst.*

## 4. Conclusion

Precipitated Y-doped ZnO nanoparticles with yttrium molar percentage values ranging from 0 to 5% were synthesized. Then, the nanoparticles were used as photocatalysts to demonstrate methylene blue degradation. The particle size of pure ZnO is 113.77±33.26 nm, which is reduced to less than one-third for the Y-doped ZnO samples. The decrease in particle size is consistent with the small crystalline size, due to low crystallization in the presence of yttrium doping. However, the expansion of the crystal structure is observed because $Zn^{2+}$ was substituted by the $Y^{3+}$. The chemical surface structures point to the major vibration of ZnO. However, some carbon-relating groups remain to appear.

The optical property reveals similar trends for all Y-doped ZnO. However, the estimated $E_g$ is reduced to the minimum value for the 4 mol% of yttrium doping condition. For the photocatalytic degradation of methylene blue, the appropriate Y-doped ZnO photocatalyst for 4 mol% yttrium doping presents the best degradation efficiency of 61.19% after photocatalytic degradation for 150 min under UV irradiation. The improvement in photocatalytic degradation is caused by the synergy of the decreased particle size and reduced $E_g$. Therefore, yttrium plays a role to decrease particle size and reduce $E_g$ of Y-doped ZnO materials, thus leading to enhance photocatalytic performance.

### Acknowledgments

This work was supported by the Kasetsart University Kamphaeng Saen Campus (grant number KPS-RDI 2019-002); the Research Promotion and Technology Transfer Center (RPTTC), Faculty of Liberal Arts and Science, Kasetsart University Kamphaeng Saen Campus (grant number 204/2564); and the Department of Physics, Faculty of Liberal Arts and Science, Kasetsart University Kamphaeng Saen Campus (grant number PHY-2021/09). The authors would like to kindly acknowledge the Department of Physics, Faculty of Liberal Arts and Science, Kasetsart University Kamphaeng Saen Campus for facility support.

## References

[1] S. K. Ray, J. Cho, J. Hur, Journal of Environmental Management **290**, 112679 (2021).
[2] Y. Sun, S. Xu, J. Y. Zeng, S. S. Yang, Q. R. Zhao, Y. Yang, Q. Zhao, G. X. Wang, Digest Journal of Nanomaterials and Biostructures **16**, 239 (2021).
[3] S. Dursun, İ. C. Kaya, M. Kocabaş, H. Akyildiz, V. Kalem, International Journal of Applied

Ceramic Technology **17**, 1479 (2020).
[4] H. Bozetine, S. Meziane, S. Aziri, N. Berkane, D. Allam, S. Boudinar, T. Hadjersi, Bulletin of Materials Science **44**, 64 (2021).
[5] S. Phophayu, P. Pimpang, S. Wongrerkdee, S. Sujinnapram, S. Wongrerkdee, Journal of Reinforced Plastics and Composites **39**, 81 (2020).
[6] M. E. Mehr, H. Maleki-Ghaleh, M. Yarahmadi, M. Kavanlouei, M. H. Siadati, Journal of Alloys and Compounds **882**, 160777 (2021).
[7] M. Saflou, S. Allahyari, N. Rahemi, M. Tasbihi, Journal of Environmental Chemical Engineering **9**, 105268 (2021).
[8] L. Huang, D. Bao, J. Li, X. Jiang, X. Sun, Applied Surface Science **555**, 149696 (2021).
[9] F. Gao, J. Yuan, X. Huang, R. Lei, C. Jiang, J. Zhuang, P. Liu, Chemical Engineering Journal **416**, 129159 (2021).
[9] F. Yu, F. Tian, H. Zou, Z. Ye, C. Peng, J. Huang, Y. Zheng, Y. Zhang, Y. Yang, X. Wei, B. Gao, Journal of Hazardous Materials **415**, 125511 (2021).
[10] L. Wang, Z. Ji, J. Lin, P. Li, Materials Science in Semiconductor Processing **71**, 401 (2017).
[11] S. Wongrerkdee, S. Moungsrijun, S. Sujinnapram, S. Krobthong, S. Choopun, Bulletin of Materials Science **42**, 91 (2019).
[12] S. Krobthong, S. Nilphai, S. Choopun, S. Wongrerkdee, Digest Journal of Nanomaterials and Biostructures **15**, 885 (2020).
[13] P. Suttiyarak, S. Buathet, A. Tubtimtae, Optik **212**, 164662 (2020).
[14] S. Sujinnapram, S. Nilphai, S. Moungsrijun, S. Krobthong, S. Wongrerkdee, Digest Journal of Nanomaterials and Biostructures **16**, 317 (2021).
[15] K. Choudhary, R. Saini, G. K. Upadhyay, V. S. Rana, L.P. Purohit, Materials Research Bulletin **141**, 111342 (2021).
[16] S. Anandan, S. Muthukumaran, Optical Materials **35**, 2241 (2012).
[17] D. B. Priya, D. Thirumalai, I. V. Asharani, Journal of Materials Science: Materials in Electronics **32**, 9956 (2021).
[18] M. Javed, M. A. Abid, S. Hussain, D. Shahwar, S. Arshad, N. Ahmad, M. Arif, H. Khan, S. Nadeem, H. Raza, S. M. Harron, Digest Journal of Nanomaterials and Biostructures **15**, 1097 (2020).
[19] C. Rodwihok, D. Wongratanaphisan, T. V. Tam, W. M. Choi, S. H. Hur, J. S. Chung, Applied Sciences **10**, 1697 (2020).